Volumetric imaging with an amplitude-steered array

Catherine H. Frazier[a)]
Bioacoustics Research Laboratory, Department of Electrical and Computer Engineering, University of Illinois at Urbana-Champaign, Urbana, Illinois 61801

W. Jack Hughes[b)]
Applied Research Laboratory, The Pennsylvania State University, P.O. Box 30, State College, Pennsylvania 16801

William D. O'Brien, Jr.[c)]
Bioacoustics Research Laboratory, Department of Electrical and Computer Engineering, University of Illinois at Urbana-Champaign, Urbana, Illinois 61801

(Received 12 August 2000; revised 13 June 2002; accepted 26 June 2002)

Volumetric acoustic imaging is desirable for the visualization of underwater objects and structures; however, the implementation of a volumetric imaging system is difficult due to the high channel count of a fully populated two-dimensional array. Recently, a linear amplitude-steered array with a reduced electronics requirement was presented, which is capable of collecting a two-dimensional set of data with a single transmit pulse. In this study, we demonstrate the use of the linear amplitude-steered array and associated image formation algorithms for collecting and displaying volumetric data; that is, proof of principle of the amplitude-steering concept and the associated image formation algorithms is demonstrated. Range and vertical position are obtained by taking advantage of the frequency separation of a vertical linear amplitude-steered array. The third dimension of data is obtained by rotating the array such that the mainlobe is mechanically steered in azimuth. Data are collected in a water tank at the Pennsylvania State University Applied Research Laboratory for two targets: a ladder and three pipes. These data are the first experimental data collected with an amplitude-steered array for the purposes of imaging. The array is 10 cm in diameter and is operated in the frequency range of 80 to 304 kHz. Although the array is small for high-resolution imaging at these frequencies, the rungs of the ladder are recognizable in the images. The three pipes are difficult to discern in two of the projection images; however, the pipes separated in range are clear in the image showing vertical position versus range. The imaging concept is demonstrated on measured data, and the simulations agree well with the experimental results.
 [DOI: 10.1121/1.1518698]

PACS numbers: 43.30.Yj, 43.30.Wi [DLB]

I. INTRODUCTION

Volumetric imaging is of interest in sonar and other applications because of the additional information provided by the third dimension of data. Three-dimensional sonar imaging has been developed for applications such as fish counting, mine hunting, and inspecting structures. In general, systems are designed to complement or replace optical systems, which are ineffective in turbid water.

Several of the systems discussed in the literature are based on transmitting a single pulse with a broad region of coverage and then focusing or processing the received signals to produce an image. Jones[1] uses a conceptually simple system, transmitting a chirp over a broad region and then using a sparse two-dimensional array to steer and focus the receive beam. The broad transmit beam lowers the achievable resolution. Such a system also suffers from poor signal-to-noise ratio due to the broad spread of transmitted energy and the high average sidelobe level of the receive beam pattern.

Murino *et al.* also use a single transmit pulse to insonify a region and a two-dimensional transducer array to receive reflected signals; however, the processing is not conventional beamforming of the received signals.[2] Instead, the processing involves a noncoherent correlation of the received signals, or correlation of the envelopes of the received signals. The proposed method is reported to have the advantages of reduction in speckle and no grating lobes regardless of interelement spacing. Thus, the array can be sparse to reduce complexity. However, it is acknowledged that the method will have poor angular resolution. In addition, although the −3-dB beamwidth of the correlation system can be made comparable to that of a focused beamforming system, the −10-dB and −20-dB beamwidths of the correlation system are much larger than those of the focused beamforming system, leading to poor image contrast.

Papazoglou and Krolik[3] have improved an imaging system for studying zooplankton by using adaptive beamforming. The original system, referred to as *FishTV*, uses two linear arrays of eight elements each in the typical geometry of a Mills Cross array. The composite pattern has 64 pencil

a)Electronic mail: hillsley@brl.uiuc.edu. Current address: Johns Hopkins University Applied Physics Laboratory, 11100 Johns Hopkins Road, Laurel, MD 20723.
b)Electronic mail: wjh2@psu.edu
c)Electronic mail: wdo@uiuc.edu

beams. A minimum variance distortionless response beamformer is used to lower sidelobes from −10 dB to −20 dB and improve resolution from 2° to 0.25°. The frame rate is reported to be 4 frames per second. Images contain few pixels and are difficult to interpret.

Other researchers are developing lens-based systems. Belcher has developed three small, high-frequency sonars that use lenses.[4,5] The transmitter is a single element or row of the two-dimensional array. The receiver is the two-dimensional array located in the focal plane of the lens. Erikson *et al.* are developing an acoustic camera. It is also a lens-based system using a transducer hybrid array (THA) and a C-scan format for data collection.[6] A separate transmitter, with a wide beam, is used to insonify the region of interest. Then, an acoustic lens is used to image multiple planes onto the acoustic array. In all of these systems, the lens accomplishes the focusing, so that the electronics requirement is reduced. A small number of range planes can be collected with a single transmit pulse; more range planes are collected with successive pulses. The total range depth that can be imaged is determined by the depth of focus of the acoustic lens, which is limited.

Recently, a linear amplitude-steered array was presented that is capable of collecting a two-dimensional set of data with a single transmit pulse and has a reduced requirement for electronics.[7] The linear amplitude-steered array steers the mainlobe by changing frequency. The potential for beam steering and imaging by changing frequency had been recognized by Lizzi and Weil.[8] Using a curved transducer with tapered thickness and exciting the transducer with different frequencies, beams with different origins and steering directions are radiated. By changing the frequency continuously, the beam is scanned through a sector. The system is limited by the fact that the ratio of highest to lowest excitation frequency cannot be more than 3. Otherwise, at the highest frequencies, multiple beams will be radiated with different orientations and steering directions, as the transducer will radiate from all places where the excitation frequency is an odd multiple of a half wavelength of thickness.

The concept of steering the maximum response of an array using amplitude weighting was introduced by Hughes and Thompson in 1976.[9] At that time, the intent of amplitude steering was to tilt the maximum response of the beam pattern without using phase-shift networks or multiple delay lines, which are bulky. A steered beam was achieved by summing the signals from two appropriately weighted subarrays with a single 90° phase shift. Initially, amplitude weighting was applied with an electronic gain,[10] but as shaped hydrophones were developed,[11] amplitude weighting was achieved geometrically, further reducing the electronics requirement.[12]

In the original formulation, the beam was steered to a particular direction at a single frequency, and the fact that the steering direction changed with frequency was considered a drawback of the design. By operating a vertical linear amplitude-steered array in broadband mode, with an impulsive or chirp excitation, the maximum response axis is swept over a range of vertical steering angles. A vertical plane of data is created from a received signal using a short-time Fourier transform (STFT). The temporal position of the STFT window gives the range of the target, and the frequencies contained within the window give the vertical angle of the target.

There have not been any experimental tests for this new volumetric imaging concept using amplitude steering. In this study a small experimental array, which was used for the low-frequency validation of the two-dimensional amplitude-steering concept, is utilized for the three-dimensional volumetric imaging. It would have been preferable to have a large aperture array with random element assignments, but one was not available. Another contribution[13] that introduced this new imaging method had demonstrated feasibility with simulated data, not experimental results. Despite the shortcomings of this array, and the fact that resolution of the images is low, the experimental results verify the simulations and support the work in the higher frequency medical imaging.

In order to collect volumetric data with a linear amplitude-steered array, the array is rotated such that the mainlobe is mechanically steered in the azimuthal direction and one pulse is transmitted for each steering direction. Data are collected in a water tank and images of three targets are produced. Section II gives a description of the array used for data collection. The experimental system used to collect the data is described in Sec. III. The image formation algorithms are briefly discussed in Section IV. And, in Sec. V, results are compared to simulations formed using the FIELD II program.[14,15] FIELD II has been widely used for simulations of transducer beam patterns and for simulations of imaging scenarios.[16–18] Following the comparison of images from simulated and experimental data, a conclusion is given.

II. DESCRIPTION OF THE ARRAY

Amplitude steering using a linear array has been described previously.[7,9,12,19] It is reviewed here briefly. The array pattern for a steered linear array with an even number of point sources/receivers can be written as

$$
\begin{aligned}
H(\theta) = \frac{2}{N}[&\cos\phi\cos u \\
&+\cdots+\cos((2n-1)\phi)\cos((2n-1)u) \\
&+\cdots+\cos((N-1)\phi)\cos((N-1)u) \\
&+\sin\phi\sin u+\cdots+\sin((2n-1)\phi)\sin((2n-1)u) \\
&+\cdots+\sin((N-1)\phi)\sin((N-1)u)] \quad n=1,...,N/2,
\end{aligned}
\tag{1}
$$

where θ is the angular position in the field, N is the (even) number of elements, d is the interelement spacing, k is the wave number at the operating frequency, k_0 is the wave number at the designed frequency, θ_0 is the designed steering angle, and $\phi=(k_0 d/2)\sin\theta_0$ and $u=(kd/2)\sin\theta$. Equation (1) is interpreted as beam steering by amplitude weighting the elements. Steering by amplitude weighting is accomplished using two sets of weightings, one phase symmetric and one phase antisymmetric. In the phase-symmetric case, the weights on each element are $\cos((2n-1)\phi)$, where

$n \epsilon [-(N/2)+1, N/2]$ is an index used to enumerate the elements. Elements placed symmetrically about the center of the array are added with equal weights and in phase. In the phase-antisymmetric case, the weights on each element are $\sin((2n-1)\phi)$. Elements placed symmetrically about the center of the array are added with equal weights and with a 180° phase shift. The output signal of the phase-antisymmetric array must be phase shifted by 90° before combining with the output of the phase-symmetric array in order to achieve the steered beam. The parameter ϕ is a fixed value as defined above. By changing the frequency, the steering angle of the mainlobe is changed as

$$\phi = \frac{k_0 d}{2} \sin \theta_0 = \frac{k_f d}{2} \sin \theta_f, \tag{2}$$

$$\theta_f = \sin^{-1}\left(\frac{f_0}{f} \sin \theta_0 \right), \tag{3}$$

where the subscript f has been added to emphasize the new operating frequency, and θ_f is the new steering direction.

The amplitude weighting can be achieved geometrically rather than electronically by dividing the available area of a single piezoelectric crystal into cosine and sine regions according to the ratio of the weights, as shown by Fig. 1. To derive this figure, we first imagine that we can phase a continuous rectangular transducer to steer its main beam. We use the following equation to determine the phase at each point along the length of the transducer:

$$H_{\text{continuous}}(\theta) = \int e^{jk_0 x \sin(\theta_0)} e^{-jkx \sin(\theta)} dx, \tag{4}$$

where θ is the angular argument of the beam pattern measured relative to the broadside direction, k_0 is the wave number at the design frequency, θ_0 is the design steering angle, and x is the spatial position along the transducer. We separate the phase into its real and imaginary parts to obtain

$$H_{\text{continuous}}(\theta) = \int \cos(k_0 x \sin \theta_0) e^{-jkx \sin \theta} dx + j \int \sin(k_0 x \sin \theta_0) e^{-jkx \sin \theta} dx, \tag{5}$$

where the first term of the sum corresponds to the cosine array and the second term corresponds to the sine array.

Part (a) of Fig. 1 shows the regions belonging to the cosine and sine arrays for the continuous transducer. The solid line represents the cosine array, and the dashed line represents the sine array. The weighting is achieved by changing the shape of the transducer. In part (b) of Fig. 1, we show that the two different weightings must occupy the same space. In Fig. 1(c), we show that the correct weighting at each x is achieved by using a cosine function and a (sine +cosine) function for weighting.

The array used in these experiments is a two-dimensional matrix of elements with elements assigned to sine or cosine regions, corresponding approximately to the regions shown in Fig. 1. The cosine and sine weightings can be positive or negative; therefore, there are four possible subgroups of elements: positive and negative cosine, and positive and negative sine. Figure 2 shows the layout of the

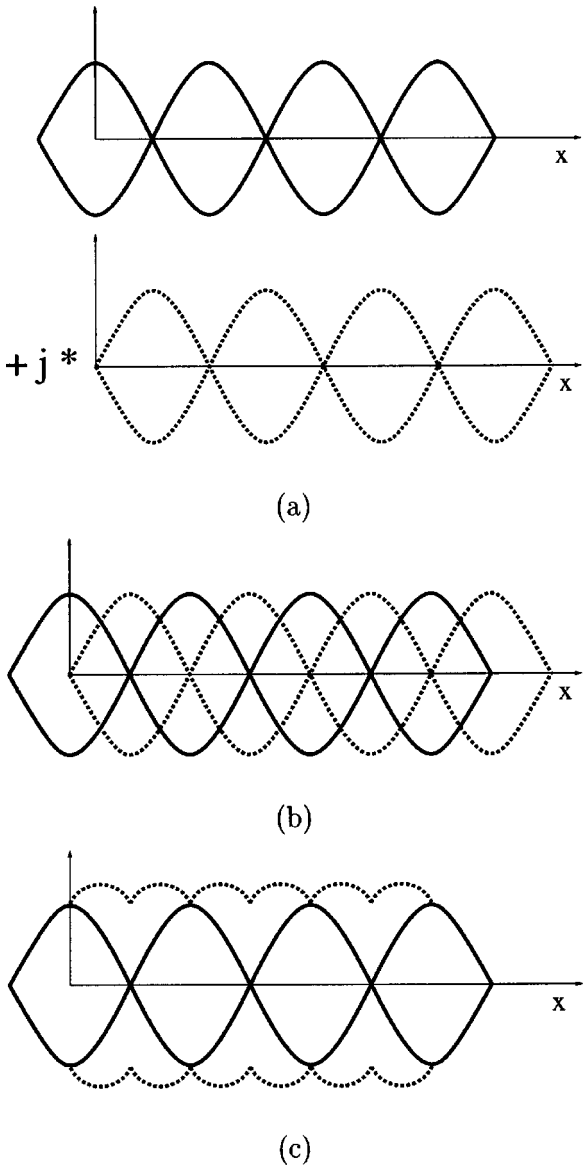

FIG. 1. Array layout for linear array. (a) The cosine (solid line) and sine (dashed line) phased elements. (b) Cosine and sine phased elements must share space. (c) In the linear array the sharing is calculated using cosine and (sine+cosine) functions.

array with four gray levels representing four subgroups of elements. In Fig. 1, the frequency separation is in the horizontal direction, and in Fig. 2, the frequency separation is in the vertical direction. Although the array layout is largely based on the ''shaped crystal'' implementation, the flexibility offered by using a matrix of elements rather than a single crystal is used to increase the intermixing of the types of elements.

The array used for data collection is approximately circular with a diameter of 10 cm. The maximum array dimensions are 52 by 55 elements. Interelement spacing is 2.11 mm in both the vertical and horizontal directions. The array has a geometric focus at 0.61 m formed by curving the array slightly; however, the focus does not have much effect as it is very close to the near-field/far-field transition even at the highest frequencies used. The array was built for purposes other than imaging, but has been used for this work to demonstrate the volumetric imaging concept on measured data.

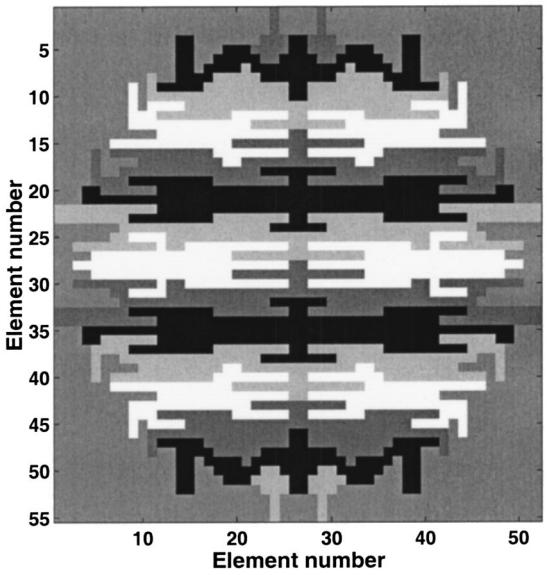

FIG. 2. Array layout for 2D array based on implementation of linear array. Four gray-scale levels represent the four phases for elements: white, cosine; black, negative cosine; light gray, sine; dark gray, negative sine.

The array is designed to steer to 30° at 100 kHz. The peak frequency response of the array is at 220 kHz. In Fig. 3, the calculated beam pattern is shown for 400 kHz. The 400 kHz beam is steered to approximately 7°. Additional major lobes appear at 49.8° in the vertical direction and ±1.59° in the horizontal direction, and they are only 12.4 dB below the mainlobe. The presence of high sidelobes reveals that this array layout or assignment of elements is nonideal. A discussion of how the beam pattern will be improved by changing the layout of the array is included in Ref. 13. Grating lobes are eliminated by randomizing the assignment of elements of different types, and the mainlobe width is improved by increasing the frequency while keeping the array diameter the same.

III. DATA COLLECTION SYSTEM

The data were collected in an anechoic tank at the Applied Research Laboratory (ARL) at the Pennsylvania State University. The tank measured 5.49 m deep by 5.33 m long by 7.92 m wide and was filled with stale water. The array

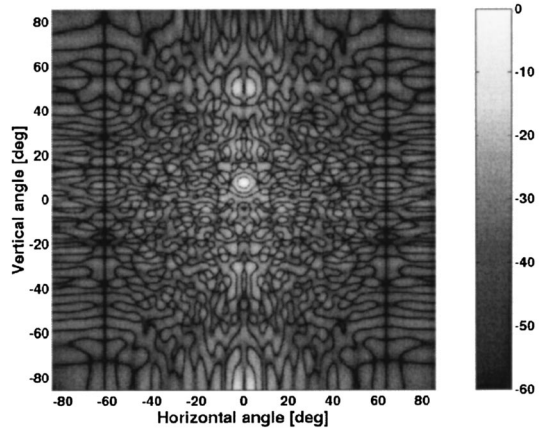

FIG. 3. Field pattern for 2D array based on implementation of linear array.

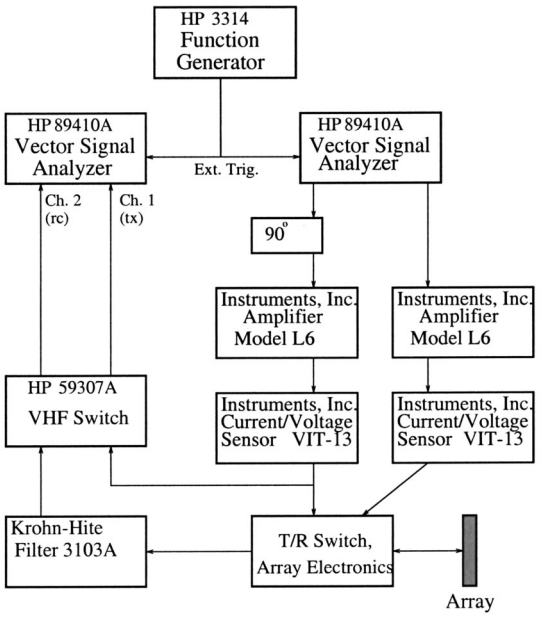

FIG. 4. Diagram of data acquisition system.

was held by a custom-built positioning system (Scientific-Atlanta, Inc., Atlanta, GA) with 0.318 cm (1/8-in.) depth resolution and ±0.02° rotational resolution around a vertical axis. Data were collected in 1° rotational steps.

A diagram of the system used to collect pulse–echo data is shown in Fig. 4. An HP 3314 function generator was used to manually trigger data collection. The transmit signal was generated by an HP 89410A vector signal analyzer. The transmit signal was split so that one signal path proceeded through a 90° phase shift to produce the excitation signal for the elements designated as sine elements. Each signal path then went through a power amplifier (model L6, Instruments, Inc., San Diego, CA). The output from each amplifier was fed into a current voltage sensor (model VIT-13, Instruments, Inc., San Diego, CA), used to monitor the current and voltage into the array electronics. The outputs from both sensors were input into the custom-built phased array electronics box (ARL), which excited the amplitude-steered array. The output from one current voltage sensor was also fed into an HP 59307A VHF switch so that the transmit voltage could be recorded by a second HP 89410A vector signal analyzer.

The received signal from the amplitude-steered array was returned back through the phased array electronics, through a Krohn-Hite 3103A filter with a passband between 500 Hz and 1 MHz, to the VHF switch, and finally to channel 2 of the second vector signal analyzer. The vector signal analyzer digitized both transmit and receive signals at a sampling rate of 1.024 MHz. Signals were stored on disk in HP format and later converted to MATLAB format using software provided by HP.

The transmit signal generated by the first vector signal analyzer is a linear FM chirp, 0.5 ms in length. The start frequency is 304 kHz and the stop frequency is 80 kHz, giving angular coverage from 9.5° to 38.7°. The lower frequencies are given greater initial amplitude to partially compensate for the frequency response of the transducer. The

array is oriented such that lower frequencies are steered farther downward than higher frequencies.

In order to process the signals, the received signals from each horizontal steering direction were first time gated to remove the initial bleed-through of the transmit. Then, the signals were filtered with a matched filter for pulse compression. The two-dimensional matrix of data contains one time signal for each azimuthal steering direction. For a complete set of volumetric data, we then apply time–frequency processing to the time signal from each azimuthal steering direction to determine vertical position and range. The STFT window is a 0.02-ms Hanning window.

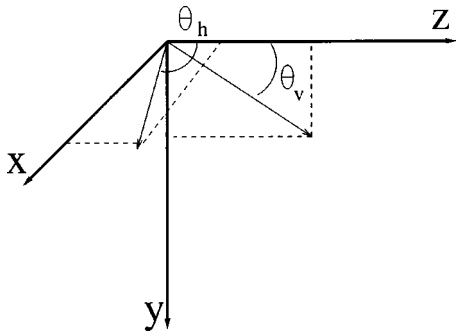

FIG. 5. Illustration to show axes and angles used to define target positions.

IV. IMAGE FORMATION ALGORITHMS

Once the three-dimensional data set has been calculated, the data must be displayed. Surface or volume rendering requires significant processing. Surface rendering is difficult when targets have flat surfaces with significant reflectivity because reflected energy may be directed away from the receiver, resulting in a low received signal despite the presence of a surface. Surface rendering also may be particularly difficult in the presence of noise or when resolution is not high enough.

Kamgar-Parsi *et al.*[5] studied many possible alternatives to volume and surface rendering including range images that display the first maximum above a threshold, and acoustic photographs which integrate the backscatter intensities along each beam. They found that displaying the maximum produced images similar to surface rendering. Taking the depth to the first maximum produced better results. These methods are limited to displaying the data at one orientation.

Projection images are another alternative to surface or volume rendering. Projection images integrate through one dimension to display the other two as an image, in which brightness indicates target strength. An image of vertical versus horizontal position is formed by summing through the range information. An image of range versus horizontal position is formed by summing through the vertical position information. And, an image of vertical position versus range is formed by summing through the horizontal information.

One way to form projection images is to begin with the full three-dimensional volume of data and sum through the various directions; however, in our case projection images are formed more directly from the received signals. Forming the three-dimensional data set requires time–frequency processing for each horizontal beam. The projection images can be formed faster using different processing. The projection image of range versus horizontal position is formed by envelope detecting the received signals from each horizontal steering direction. Range resolution is better than time–frequency methods that use a sliding window, effectively averaging over the samples in the window. The image of vertical position versus horizontal position is formed by taking a single Fourier transform of the entire received signal for each steering direction. Since the image does not display any range information, time–frequency processing is not necessary for this image. Also, by using the entire signal, the best frequency resolution is obtained, giving the best resolution of vertical position. These two images represent the extremes of using the STFT, with very short or very long processing windows. Finally, to form the image of vertical position versus range, time–frequency processing is required. Rather than performing the calculation for every horizontal beam, the sum through the horizontal beams is taken first, and then the time–frequency distribution is calculated only once.

The image resolution is dependent not only on the size of the array,[7] but also on the processing used to form the images. Also, because of the frequency separation, resolution will vary throughout the insonified field. Following the analysis of Ref. 7, which defines resolution as the -3-dB width of the point spread function, the best range resolution we could achieve is $0.4423c/\Delta f$, which corresponds to 3.0 mm. The best lateral resolution we could achieve is 4.4 cm at 304 kHz and 16.6 cm at 80 kHz at a range of 1 m. Image formation algorithms are described in greater detail in Ref. 19.

V. SIMULATED AND EXPERIMENTAL RESULTS

Pulse–echo data were collected for several targets using the system described above. To describe target locations, we give two sets of coordinates, which are pictured in Fig. 5. The first set of coordinates is in (x,y,z) form, where x is the horizontal position parallel to the face of the array, y is the depth, and z is the horizontal position perpendicular to the face of the array. Thus, x and y are lateral positions and z is an axial position. Positive y is down, and positive z is away from the array in the broadside direction. Positive x follows from the right-hand rule. This convention is in agreement with that used by the FIELD II program.

The second set of coordinates is in (r,θ_v,θ_h) form, where r is the range from the center of the array, θ_v is the vertical angle relative to horizontal with the origin at the center of the array, and θ_h is the horizontal angle relative to the broadside direction, also with the origin at the center of the array. Both sets of coordinates are given because the images of the targets are given using both coordinates.

In the simulations, the frequency response of the transducer was assumed to be flat, and the excitation signal did not change amplitude with frequency. The target positions were rotated to simulate the rotation of the array. Processing of the simulated data was the same as processing of the experimental data, with the exception of the initial time gating, which was not necessary for the simulated data.

Comparisons between the simulations and experiments are made on a qualitative basis. Target positions were measured at the water surface and therefore are known only approximately. Gross differences between the images from simulated and experimental data are apparent visually. Numerical comparisons, for example using the energy of a difference image or a correlation technique, would require multiple time-consuming simulations as the targets are translated and rotated to provide a better match, and not much insight would be gained.

A. Ladder target

The ladder target was a standard 6-ft. wooden step ladder with rungs that were 30.5 cm (1 ft.) apart. The ladder was placed in the water in the folded position so that it hung approximately vertically, 1.2 m away from the array. Figure 6(a) shows a picture of the target and array. The target position and orientation are shown in Fig. 6(b). Two rungs appear within the insonified region; however, a third rung is very close in depth to the insonified region. The locations of these three rungs are given by the coordinates ($\pm$0.152 m, 0.406 m, 1.2 m); ($\pm$0.152 m, 0.711 m, 1.2 m); and ($\pm$0.152 m, 1.02 m, 1.2 m). In terms of angles, the coordinates are (1.27 m, 18.7°, $\pm$7.2°); (1.40 m, 30.7°, $\pm$7.2°); and (1.57 m, 40.2°, $\pm$7.2°). The positive and negative values in the x and θ_h coordinates represent a range which is the extent of a rung. Data were collected over a range of horizontal angles from $-30°$ to 30°. In the simulation, the sides of the ladder and each rung were represented as a line of point targets. To represent the targets, 53 636 points were used.

Figure 7 shows the projection images through the vertical angle using simulated and experimental data. The three rungs should be present at 1.27, 1.4, and 1.57 m. All three rungs are visible at the correct ranges in the image from simulated data. The farthest rung is less bright because it is not fully within the insonified region. Preceding the closest rung in range, there is a very thin line that extends across the image. This artifact is due to the discontinuity at the onset of the received signal. The artifact is also present in the image from experimental data, to a lesser extent. The third rung is not visible in the image from experimental data, due to the low response of the array at lower frequencies, and due to the position of the rung just outside of the insonified region. At the closest/highest rung, reflections from the sides of the ladder appear. Also, there is an additional reflection at the top rung in the experimental data probably due to the fact that the ladder is a folding ladder, and there is a step behind the rung.

Figure 8 shows the projection images through range using simulated and experimental data. Both the image from simulated data and the image from experimental data show two rungs. The third rung is below the range shown in the image. The upper rung appears smaller, indicating the smaller beamwidth at the higher frequency. In both cases, the lower rung appears wider. In the image from experimental data, the lower rung also appears less bright, due to the smaller response of the transducer at the lower frequency.

Figure 9 shows the projection images through the horizontal angle using simulated and experimental data. Both the images from simulated and experimental data show three rungs. The highest rung appears to be closest to the transducer in range. The third (lowest) rung appears in this projection because summing across the horizontal angles has increased the signal level above the threshold for display. However, only part of the lowest rung is visible. The middle rung appears the brightest because of the summing operation. The simulated image is very smooth. There is a reflection that extends through most of the vertical distance just before the highest rung. That reflection is due to the artifact described above caused by the onset of the signal. The image from experimental data also has a reflection before the first (highest) rung, due to the artifact. In addition, there is a reflection behind the highest rung and above the middle rung. It may be a reflection from the flat step behind the rung. Although the ladder is hanging vertically, the rungs

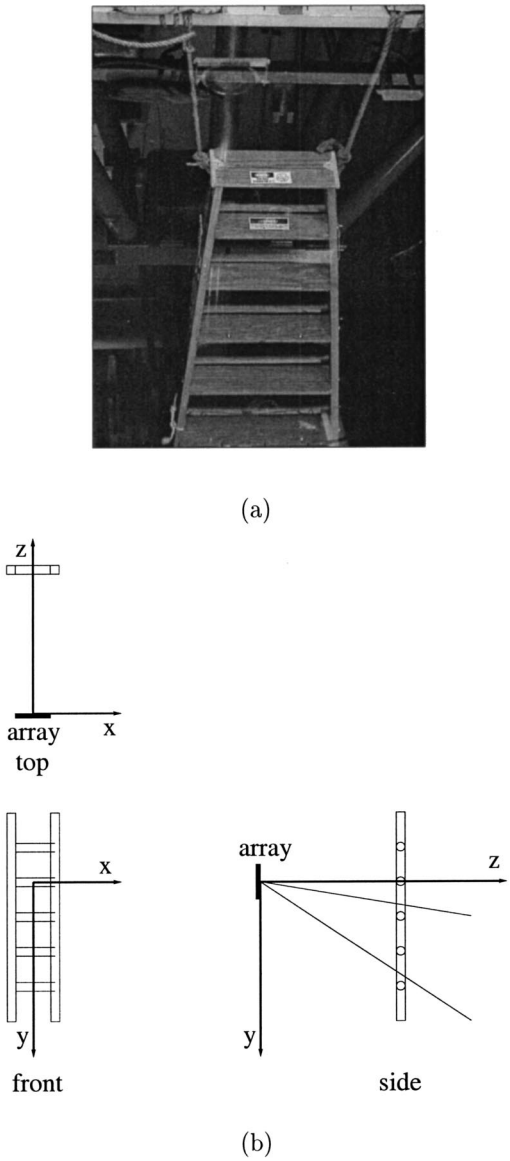

FIG. 6. (a) Picture of the ladder target prepared for data collection. The array is the circular object held by a frame behind the ladder (above the ladder in the picture.) The structure that holds the array is reflected in the water surface. (b) Top, front, and side views to show position and orientation of ladder target.

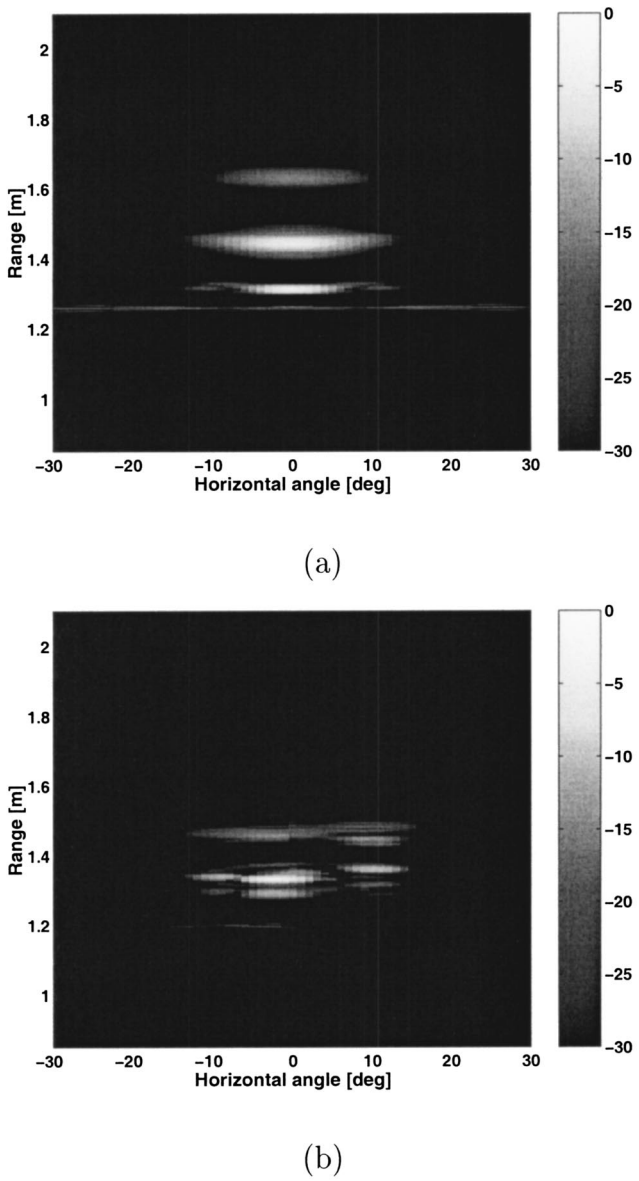

FIG. 7. Images of the ladder target [corresponding to the top view of Fig. 6(b)]. Range versus horizontal angle (a) simulated; (b) experimental. The gray scale is in dB.

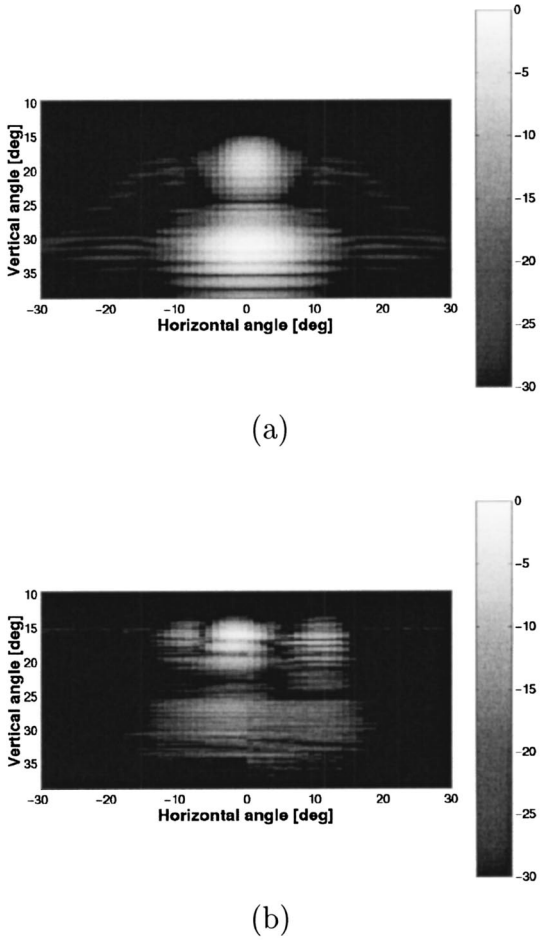

FIG. 8. Images of the ladder target [corresponding to the front view of Fig. 6(b)]. Vertical angle versus horizontal angle (a) simulated; (b) experimental. The gray scale is in dB.

appear to move away from the transducer in range as they become deeper because the insonified region is off-broadside, directed downward.

In the three images, the rungs of the ladder are clearly long in the horizontal direction and compact in the vertical and range directions. There is excellent agreement between the simulated and experimental data for these three sets of images. The rungs of the ladder are perpendicular to the direction of frequency separation, and therefore each rung reflects a small range of frequencies. There are some differences that show more structure in the experimental data due to the model of the ladder and due to the fact that the simulation assumes simple reflection.

B. Three-pipe target

The next targets used were three steel pipe targets. The pipes are each 3.05 m (10 ft.) long, with an outer diameter of 2.54 cm (1 in.) and an inner diameter of 0.794 cm (5/16 in.). The targets are arranged as three corners of a square, where the side of the square has a length of 30.5 cm (1 ft.). The target positions and orientations are shown in Fig. 10. The pipe locations are given by the coordinates (0 m, −, 1.0 m); (0 m, −, 1.305 m); and (−0.305 m, −, 1.305 m). For the pipe targets, no y coordinate (depth) is specified because the targets extend through the entire depth coverage of the array. In terms of (r, θ_v, θ_h) coordinates, the targets are at (1.0 m, −, 0°); (1.305 m, −, 0°); and (1.340 m, −, −13.15°). θ_v is the entire insonified depth of the array, 9.5° to 38°. Data were collected over a range of horizontal angles from −25° to 10°. In the simulation, each pipe was represented as a single line of points. The three pipe targets were defined by 60 003 points.

Figure 11 shows the projection through the vertical direction. In the simulated image, each pipe target appears as a very thin horizontal line. The horizontal lines extend across the whole image because the beamwidth of the lowest frequency (80 kHz) is 20°, and the image shows only a 35° sector. The image formed with experimental data agrees in character with the image formed with simulated data. The separation in range between the pipes appears to be larger than 0.305 m. This difference in separation is probably due to the pipes hanging at an angle and not perfectly vertical.

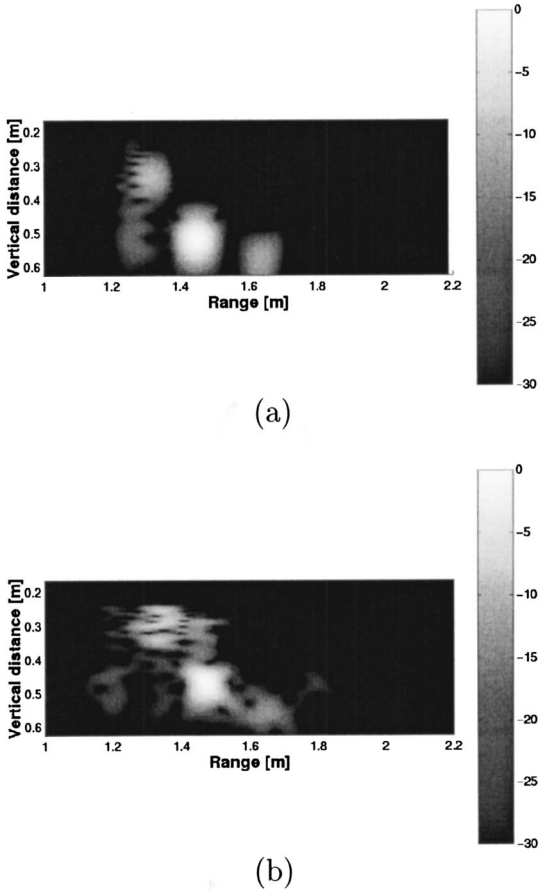

FIG. 9. Images of the ladder target formed using the STFT [corresponding to the side view of Fig. 6(b)]. Vertical angle versus range (a) simulated; (b) experimental. The gray scale is in dB.

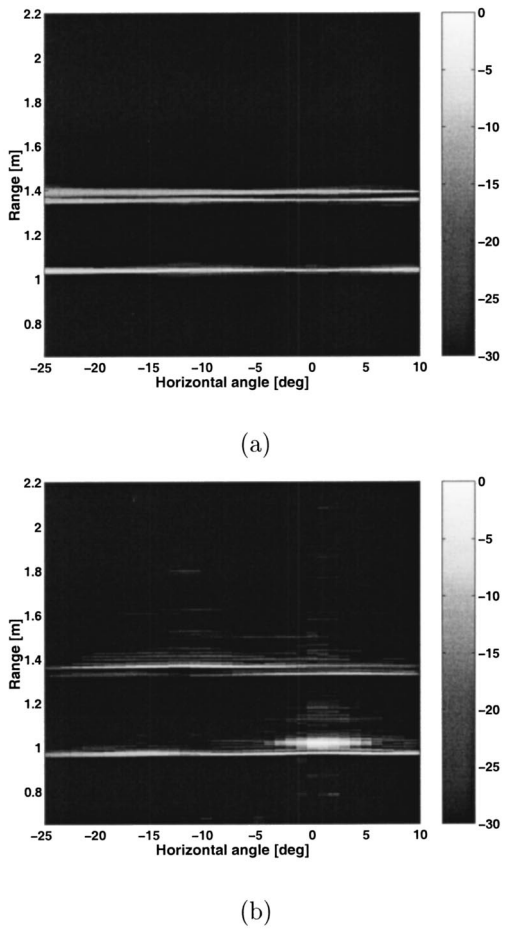

FIG. 11. Images of the three-pipes target (corresponding to the top view of Fig. 10). Range versus horizontal angle (a) simulated; (b) experimental. The gray scale is in dB.

The distances between the pipes were measured at the top of the pipes, slightly above the water level. If the pipe that is nominally at $x=0$ m and $z=1.305$ m is hanging at a 3° angle, the farther pipe in range would appear to be 0.4 m from the closer pipe, rather than 0.3 m, as expected. The image formed with experimental data also has a distinct bright spot at 0° in the horizontal direction and 1.0 m in range. This reflection is probably a particularly strong reflection from the closest pipe, perhaps due to reverberation in the pipe or a flaw in the pipe. There were no other targets in the water, and there should not have been any air trapped in the pipe.

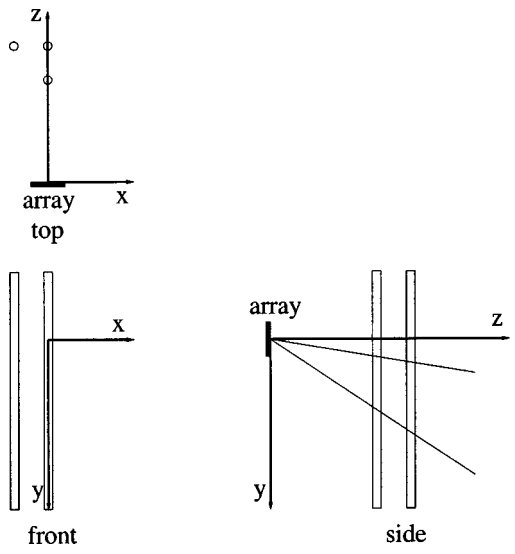

FIG. 10. Top, front, and side looks at the three-pipes targets.

Figure 12 shows the simulated and experimental results for the projection through range. Again, the images formed using simulated and experimental data are similar. In particular, both have the bright diagonal returns that fill the image. This characteristic is more noisy in the image from experimental data, and it is also less bright because of the brighter spot at 0° horizontally and 15° vertically, as discussed above. Both images are filled with reflections because the targets extend through the entire vertical region and because the beamwidths are wide in the horizontal direction, particularly at the lower frequencies which appear at the bottom of the image. Although it would be difficult to discern three pipes in this image, this image is valuable for showing that the simulations agree with the experimental data.

Figure 13 shows the simulated and experimental results for the projection through horizontal angle. Signals from $-10°$ to 10° were included in the sum to form the projection through the horizontal angle, so that signals were summed symmetrically about $\theta_h=0°$ even though the data were not collected symmetrically around the $\theta_h=0°$ angle. The im-

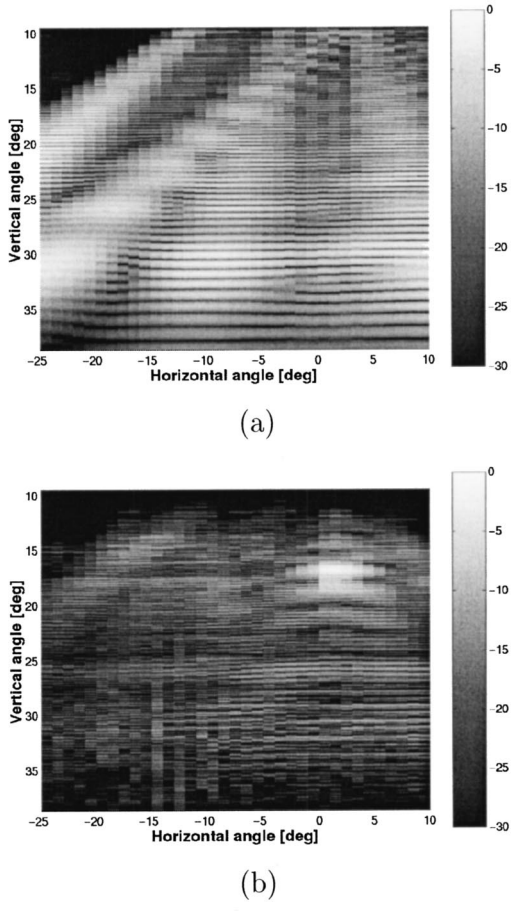

FIG. 12. Images of the three-pipes target (corresponding to the front view of Fig. 10). Vertical angle versus horizontal angle (a) simulated; (b) experimental. The gray scale is in dB.

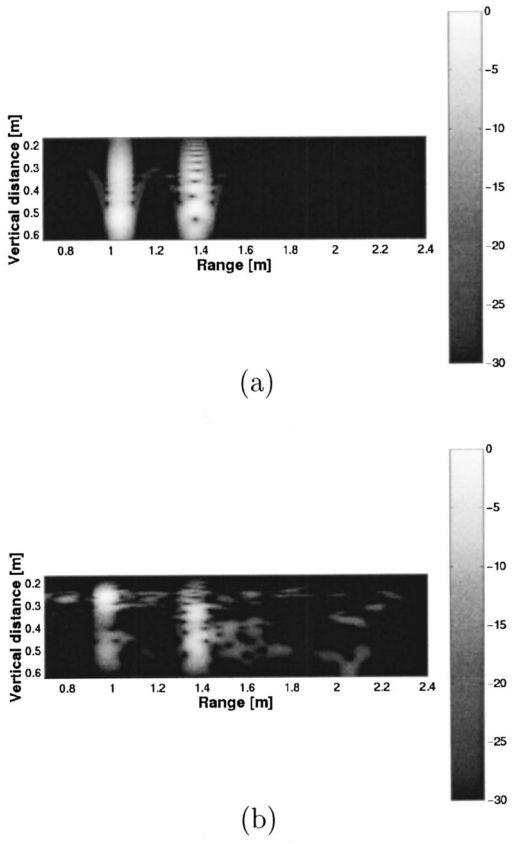

FIG. 13. Images of the three-pipes target formed using the STFT (corresponding to the side view of Fig. 10). Vertical angle versus range (a) simulated; (b) experimental. The gray scale is in dB.

ages are similar in character, showing two vertical lines, one at 1.0 m and one farther in range. The difference in range separation has been discussed previously. The two vertical lines represent the three targets. In this projection, two targets at the same range cannot be separated. In the image from simulated data, the brightest reflections occur at lower vertical distances. In the image from experimental data, the brightest reflection occurs at the top of the closer target. This location of the brightest reflection agrees with that of the other two projections for experimental data.

The images of the three pipes are poorly resolved in the horizontal direction due to the wide horizontal beamwidths of this array; however, there is good agreement between images formed with simulated and experimental data. Differences arise because of a particularly strong echo in the experimental data, although the origin of this bright echo is unknown. Horizontal beamwidths can be improved by increasing the array diameter. In this case, the array diameter is 20 wavelengths at the highest frequency and 5 wavelengths at the lowest.

VI. DISCUSSION AND CONCLUSIONS

This study demonstrates with experimental data the use of the linear amplitude-steered array for volumetric imaging on measured data. The rungs of the ladder were fairly well represented by the three projection images. The three pipes were best represented by the projection through the horizontal direction, which showed that the targets were discrete in range and extended in the vertical direction. The projection through range and through the vertical direction suffered from poor horizontal resolution, which made it difficult to see the pipe that was separated laterally from the other two.

Simulations of the array operation were confirmed with experiments conducted in the water tank at the Pennsylvania State University Applied Research Laboratory. There was excellent agreement between simulations and experiments. The three-pipes target introduced additional complexity in that the target was line-like rather than point-like in a vertical plane; however, the agreement between simulation and experimental data was still good. Hard targets with broad smooth surfaces are more difficult to represent as a collection of point targets, for the purposes of simulation, requiring large numbers of densely spaced points. The effects of shadowing must be included in the calculations. Difficulty in imaging hard smooth surfaces is a problem with acoustic imaging systems in general, in that the bulk of the energy may be reflected away from the receiver for monostatic imaging with a high angle of incidence. The amplitude-steered array is not an exception. Data collected from a water-filled aluminum shell showed a bright reflection from a particular region of the front surface and smaller reflections from each end of the cylinder, but the shape of the cylinder was not apparent in the images.

In this study, we rotated the linear array to obtain the third dimension in the data. For imaging longer ranges or for truly real-time volumetric imaging, the configuration would be modified such that the transmitted beam is broad in the horizontal direction and phased array beamforming would be used on receive in the horizontal direction to steer and focus the beam. Such an array, operating at a higher frequency is the subject of Ref. 13. In that work, the array layout is modified to lower sidelobes. The beamwidths are improved by increasing frequency while keeping the size of the array the same. Focusing is also implemented. Frequency and size of the modified array layout are chosen for a particular underwater imaging application.

ACKNOWLEDGMENTS

The authors would like to thank Mark Geleskie, Pete Tussey, and Greg Granville from the Applied Research Laboratory for collecting the data. We would also like to thank the anonymous reviewers whose comments greatly improved the presentation of this material.

[1] I. S. F. Jones, ''High resolution underwater acoustic imaging,'' in Proceedings of Oceans 1999 MTS/IEEE, 1999, pp. 1093–1097.
[2] V. Murino, C. S. Regazzoni, A. Trucco, and G. Vernazza, ''A noncoherent correlation technique and focused beamforming for ultrasonic underwater imaging: A comparative analysis,'' IEEE Trans. Ultrason. Ferroelectr. Freq. Control **41**(5), 621–630 (1994).
[3] M. Papazoglou and J. L. Krolik, ''High resolution adaptive beamforming for three-dimensional acoustic imaging of zooplankton,'' J. Acoust. Soc. Am. **100**, 3621–3630 (1996).
[4] E. O. Belcher, H. Q. Dinh, D. C. Lynn, and T. J. Laughlin, ''Beamforming and imaging with acoustic lenses in small, high-frequency sonars,'' Proceedings of Oceans 1999 MTS/IEEE **3**, 1495–1499 (1999).
[5] B. Kamgar-Parsi, B. Johnson, D. L. Folds, and E. O. Belcher, ''High-resolution underwater acoustic imaging with lens-based systems,'' Int. J. Imaging Syst. Technol. **8**(4), 377–385 (1997).
[6] K. Erikson, A. Hairston, A. Nicoli, J. Stockwell, and T. White, ''128×128 (16 K) ultrasonic transducer hybrid array,'' Acoust. Imaging **23**, 485–494 (1998).
[7] C. H. Frazier, W. J. Hughes, and W. D. O'Brien, Jr., ''Resolution analysis for an amplitude steered array,'' J. Acoust. Soc. Am. **107**, 2430–2436 (2000).
[8] F. L. Lizzi and K. W. Weil, ''Frequency-controlled scanning of ultrasound beams,'' United States Patent 4,350,917, 21 Sept. 1982.
[9] W. J. Hughes and W. Thompson, Jr., ''Tilted directional response patterns formed by amplitude weighting and a single 90° phase shift,'' J. Acoust. Soc. Am. **59**, 1040–1045 (1976).
[10] W. J. Hughes, W. Thompson, Jr., and R. D. Ingram, ''Transducer array scanning system,'' United States Patent 3,905,009, 9 Sept. 1975.
[11] W. J. Hughes and C. W. Allen, ''A shaped PVDF hydrophone for producing low sidelobe beampatterns,'' Proceedings of the 1992 Symposium on Autonomous Underwater Vehicle Technology, 2–3 June 1992, Washington, D.C.
[12] W. J. Hughes and C. W. Allen, ''A spatially phased transducer to form steered beams,'' Proceedings of SPIE, Medical Imaging 1999: Ultrasonic Transducer Engineering **3664**, 138–146 (1999).
[13] C. H. Frazier, W. J. Hughes, and W. D. O'Brien, Jr., ''A high frequency amplitude-steered array for real-time volumetric imaging,'' J. Acoust. Soc. Am. **112**, 2742–2752 (2002).
[14] J. A. Jensen, ''FIELD: A program for simulating ultrasound systems,'' Med. Biol. Eng. Comput. **34**(1), 351–353 (1996).
[15] Program is available at http://www.it.dtu.dk/~jaj/field/field.html
[16] M. E. Anderson, M. S. Soo, R. C. Bentley, and G. E. Trahey, ''The detection of breast microcalcifications with medical ultrasound,'' J. Acoust. Soc. Am. **101**, 29–39 (1997).
[17] W. F. Walker and G. E. Trahey, ''Speckle coherence and implications for adaptive imaging,'' J. Acoust. Soc. Am. **101**, 1847–1858 (1997).
[18] E. Maione, P. Tortoli, G. Lypacewicz, A. Nowicki, and J. M. Reid, ''PSPICE modeling of ultrasound transducers: Comparison of software models to experiment,'' IEEE Trans. Ultrason. Ferroelectr. Freq. Control **46**(2), 399–406 (1999).
[19] C. A. H. Frazier, ''A two-dimensional amplitude-steered array for real-time volumetric acoustic imaging,'' Ph.D. thesis, University of Illinois at Urbana-Champaign, 2000.